# Copper-Phosphonate Lamella Intermediates Control the Shape of Colloidal Copper Nanocrystals

James R. Pankhurst[a], Laia Castilla i Amorós[a], Dragos Stoian[b], Jan Vavra[a], Valeria Mantella[a], Petru P. Albertini[a], Raffaella Buonsanti[a]*

[a] Laboratory of Nanochemistry for Energy (LNCE), Institute of Chemical Sciences and Engineering (ISIC), École Polytechnique Fédérale de Lausanne (EPFL), Rue de l'Industrie 17, 1950 Sion, Switzerland

[b] The Swiss-Norwegian Beamlines, European Synchrotron Radiation Facility (ESRF), 38000 Grenoble, France

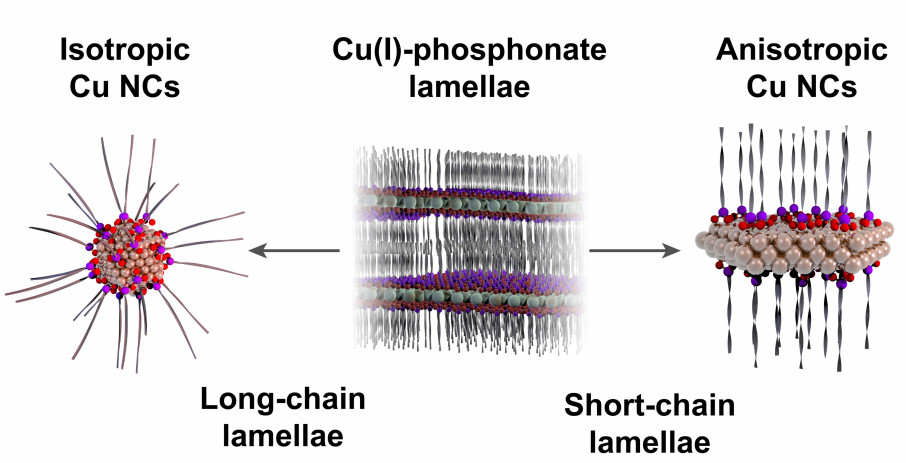


**Abstract**

Understanding the structure and behavior of intermediates in chemical reactions is key to developing greater control over the reaction outcome. This principle is particularly important in the synthesis of metal nanocrystals (NCs), where the reduction, nucleation and growth of the reaction intermediates will determine the final size and shape of the product. The shape of metal NCs plays a major role in determining their catalytic, photochemical and electronic properties and, thus, the potential applications of the material. In this work, we demonstrate that layered coordination polymers, called lamellae, are reaction intermediates in Cu NC synthesis. Importantly, we discover that the lamella structure can be fine-tuned using organic ligands of different length and that these structural changes control the shape of the final NC.

Specifically, we show that short-chain phosphonate ligands generate lamellae that are stable enough at the reaction temperature to facilitate the soft-templating of Cu nuclei into anisotropic Cu NCs, being primarily triangular plates. In contrast, lamellae formed from long-chain ligands lose their structure and form spherical Cu NCs. The synthetic approach presented here provides a versatile tool for the future development of metal NCs, including other anisotropic structures.

**Introduction**

Well-defined metal nanocrystals (NCs) offer exciting opportunities as active and functional materials in catalytic, biological, energy conversion and electronic applications.[1–5] Their size and shape modulate their properties, therefore tuning these features during their synthesis is of crucial importance.[1–5] Colloidal chemistry offers a greater level of precision and tunability along with easy processability in comparison with other synthesis methods, including those based on high-vacuum deposition techniques.[6–8] Generally speaking, in colloidal synthesis, metal precursors are mixed in a carrier solvent, often with a reducing agent, in the presence of surfactants or ligands that stabilize the final NC product.[6–8] By fine-tuning several reaction parameters, including temperature, time, atmosphere, and rate of addition of a reagent, the size and shape of the final product can be controlled.[6–8]

Classical nucleation theory describes a simplified process where the metal precursors convert directly into metal nuclei.[9] However, recent research highlights that the formation of NCs is often more complex.[10] The realization that NC formation is a multi-step process, which includes the formation of metastable pre-nucleation intermediates, opens up a greater number of possibilities to influence the reaction.[11] Specifically, the manipulation of these intermediates emerges as a strategy to control the size and shape of the final NC products.

Ligands carry out a number of roles in colloidal synthesis and drastically influence its outcome.[8,12–15] First of all, the dynamicity and strength of the ligand binding to specific crystal facets determines the rate of growth at that site and, thus, the final NC shape.[16,17] Secondly, the ligands can interact with the metal precursor itself to form reaction intermediates.[11] These intermediates span from simple molecular complexes and clusters to more complex superstructures.[11] In the former, the coordination chemistry between the metal precursor and the ligands will impact the kinetics of nucleation and growth and thus the final NC size and shape.[18–21] Insight into metal-ligand interactions in precursor complexes has been used to obtain unprecedented shape control of Cu NCs and superior size monodispersity of InP

NCs.[22,23] Coordination polymer lamellae are one example of reaction intermediates with a more complex superstructure. They are layered structures built from the self-assembly of organic ligands and metal ions.[24] The layering of the coordination polymers is promoted by the intermolecular interactions between hydrocarbon tails, in a similar way to lipid bilayers.[25–27] The coordinating functional group in the ligand, such as a sulfonate, phosphonate, thiolate or amine, is responsible for bridging multiple metal ions and forming the coordination polymer, in either one or two dimensions.[28–31] Lamellar structures incorporating metal ions or clusters have been isolated as reaction intermediates of colloidal semiconductor NCs and have enabled the synthesis of new complex architectures, including low-dimensional structures, by acting as soft templates during the growth.[32–40] A few promising examples of soft-templating exist for metal NCs, though in a much less advanced stage of development.[30,31] Generally, despite the growing interest and effort by scientists working in the field, the relationships between the chemical nature of the ligands, the structure of the reaction intermediates and the final NC products remain to be discovered.

In this work, we contribute to advancing the current knowledge of reaction intermediates in the colloidal synthesis of NCs and of the manipulation of these intermediates to target NC products with a desired shape. Specifically, we explore how different phosphonic acid ligands can be used to control the structure of lamella intermediates and how these different structures influence the reduction and growth stages in the synthesis of Cu NCs.

Cu NCs have been chosen as a model system as they are promising catalysts for the electrochemical $CO_2$ reduction reaction ($CO_2RR$).[41–48] Recent research highlights the intimate relationship between the crystallographic facets exposed by the NC catalyst and the reactivity, even beyond the $CO_2RR$.[43,46,49–52] These studies encourage the continued development of Cu NC shape control, which is still limited compared to what has been achieved for other metals.[7] Only further insight into their synthesis can drive the current state of research forward.

Herein, we combine *in-situ* X-ray absorption and diffraction techniques with *ex-situ* electron microscopy to understand the chemical and structural changes that occur during NC formation involving lamella intermediates. We highlight the significance of this approach by demonstrating that a structural modification of the reaction intermediates, driven by the chemical identity of the ligands, drastically alters the shape of the NC product, in this case switching from isotropic Cu NCs (spheres) to anisotropic Cu NCs (primarily triangular plates).

By providing insight into how lamella intermediates can be rationally controlled to target desired NC products, this study contributes to the development of synthetic schemes for metal NCs beyond trial-and-error approaches.

**Results and Discussion**

The synthesis of Cu NCs *via* lamella intermediates that we have developed makes use of copper(I) acetate (Cu(OAc)) as the copper precursor, an aliphatic phosphonic acid ligand and tri-*n*-octylamine (TOA) as the solvent and reducing agent (**Figure 1**). The reaction comprises four stages (**Figure S1**): i) a heating ramp from near room temperature to the lamella formation temperature, $T_1$; ii) a plateau at $T_1$ for 30 minutes; iii) a heating ramp from $T_1$ to the reaction temperature, $T_2$; and iv) a plateau at $T_2$ for 30 minutes. This approach was inspired by the recent discovery that spherical Cu NCs form from copper-phosphonate lamellae when Cu(OAc) reacts with *n*-tetradecylphosphonic acid (TDPA) in TOA at 270 °C.[31] In that study, the long-chain lamellae collapse into reverse micelles during heating, resulting in a size-focusing effect for the Cu spheres.[31] Instead, to make use of the lamellae as a shape-directing soft-template, the lamella structure must remain intact during the NC nucleation and growth phase.[32–40] Tuning the length of the aliphatic chain should have an important effect on the thermal stability and reduction behavior of the lamellae. However, predicting the structure of the lamellae and their thermal stability from the chemical identity of the ligands is not trivial. Multiple scenarios are indeed possible. For example, it is expected that long-chain lamellae are more thermally robust than short-chain lamellae if the aliphatic chains are fully interdigitated, as more van der Waals interactions would exist between neighboring chains.[53–55] The opposite is anticipated when only partial interdigitation between the aliphatic chains occurs. In that case, the higher structural flexibility of the long-chain lamellae would render them less stable and more prone to entropy-driven dissolution. Experiments are needed to validate one scenario over the other.

Therefore, we investigated several phosphonic acid ligands with different aliphatic tail lengths, which are drawn in **Figure 1**: *n*-tetradecylphosphonic acid (TDPA, $C_{14}$ tail); *n*-decylphosphonic acid (DPA, $C_{10}$ tail); *n*-octylphosphonic acid (OPA, $C_8$ tail); *n*-hexylphosphonic acid (HPA, $C_6$ tail); and *n*-butylphosphonic acid (BPA, $C_4$ tail).

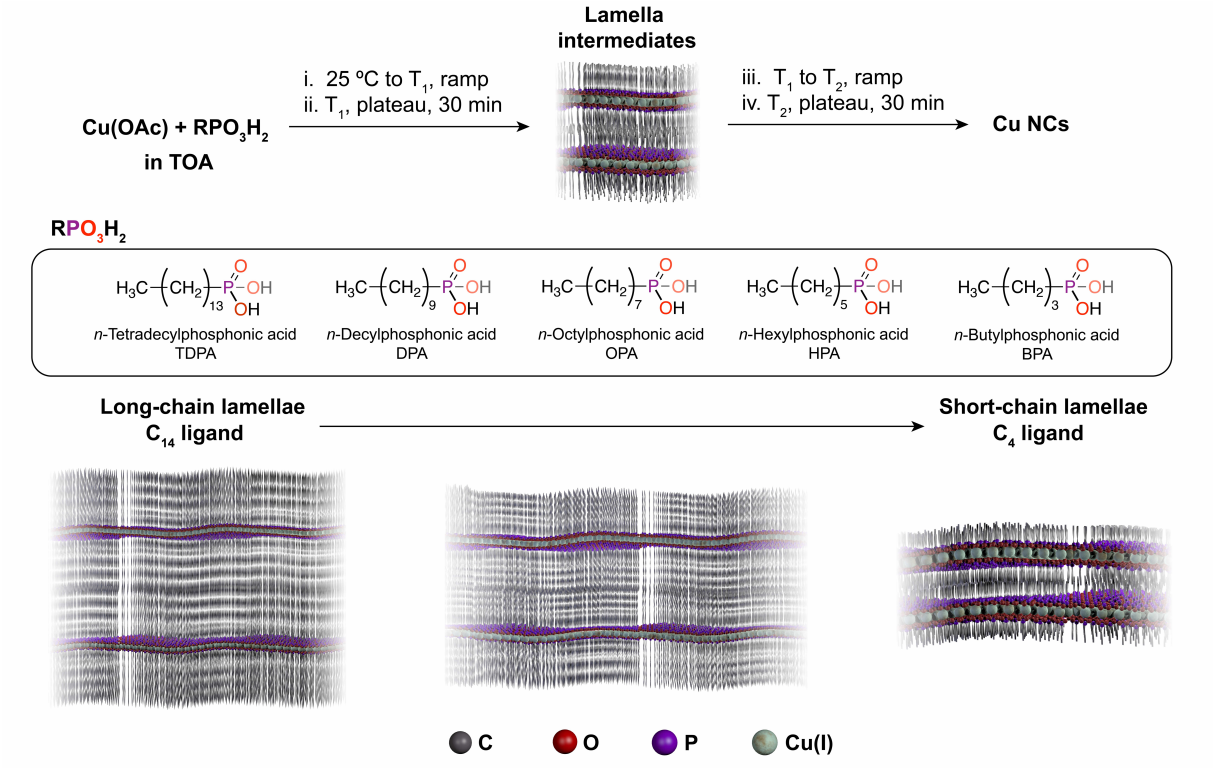


**Figure 1.** An overview of the synthesis of Cu NCs, using phosphonic acid ligands to build lamella intermediates. $T_1$ is the lamella formation temperature (typically 150 – 180 ºC); $T_2$ is the reaction temperature where Cu NCs are formed (greater than 180 ºC). The different phosphonic acids used in this work are shown in the box. A schematic representation of lamella structures with decreasing interlayer spacings is sketched at the bottom.

### *Characterization of the copper-phosphonate lamella intermediates*

To verify that all of the ligands do indeed form copper-phosphonate lamellae and to learn more about their structure, we first analyzed the intermediates that form at 150 ºC by X-ray diffraction (XRD). This temperature was chosen as the Cu-TDPA lamellae were previously detected to form during the heating ramp, between 90–160 ºC.[31] **Figure 2A** shows that lamellar structures are present in all cases and no diffraction from metallic Cu is observed. The periodic set of low-angle diffraction peaks is characteristic for lamellae and allows the interlayer spacing (*D*) to be determined. The *D* spacings that are derived from these diffraction peaks show that the interlayer distances are governed directly by the length of the phosphonic acid ligands. Indeed, the measured *D* values are in very good agreement with the distances approximated using simple molecular mechanics models of the different Cu(I)–phosphonate building blocks (**Figure 2B**). They match closely with double the length of the Cu-phosphonate unit (including the aliphatic tail), indicating that minimal interdigitation of the chains occurs. In addition, the Fourier-transform infrared (FT-IR) absorption spectra confirm that the

phosphonic acids are present in the lamella structures as fully deprotonated phosphonate ligands (**Figure S2**).

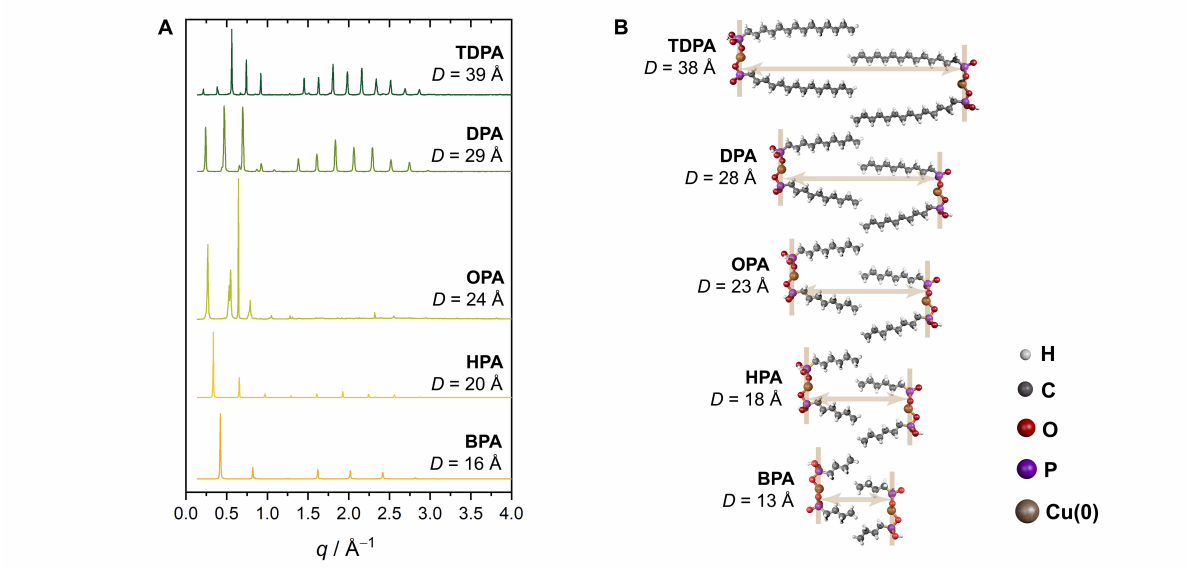


**Figure 2. A**) XRD patterns for lamella intermediates with different length phosphonic acid ligands, isolated at 150 ºC. The lamella interlayer spacings (*D*) are given for each intermediate. **B**) Molecular mechanics models for the different lamellae, used to predict the interlayer spacings, indicated by brown arrows. Details of the molecular mechanics calculations are given in the Supporting Information.

### *Effect of the phosphonic acid chain length and the reaction temperature on the morphology of the reaction product*

Having assessed that all of the ligands form lamellae, we proceeded towards investigating the products from reactions at different $T_2$ temperatures, while keeping $T_1$ at 180 ºC, which was chosen based on our previous work with Cu-TDPA.[31] **Figure 3** shows representative transmission electron microscopy (TEM) images of these products. At higher temperatures, namely 250 ºC and 270 ºC, spherical Cu NCs form regardless of the aliphatic chain length of the ligands. At intermediate reaction temperatures, between 210–230 ºC, spherical Cu NCs are still obtained with the long-chain phosphonic acid ligands TDPA and DPA, although their size dispersity is generally poorer (**Figures S3–S5**). Instead, a mixture of triangles and thinner sheets are observed for the short-chain ligands HPA and BPA. Finally, at the lowest reaction temperature of 180 ºC, very large, nebulous structures are isolated when long ligands (TDPA, DPA) were used. More discrete, yet still interconnected, globules are observed with HPA. The reaction including BPA generates distinctly 2D sheets.

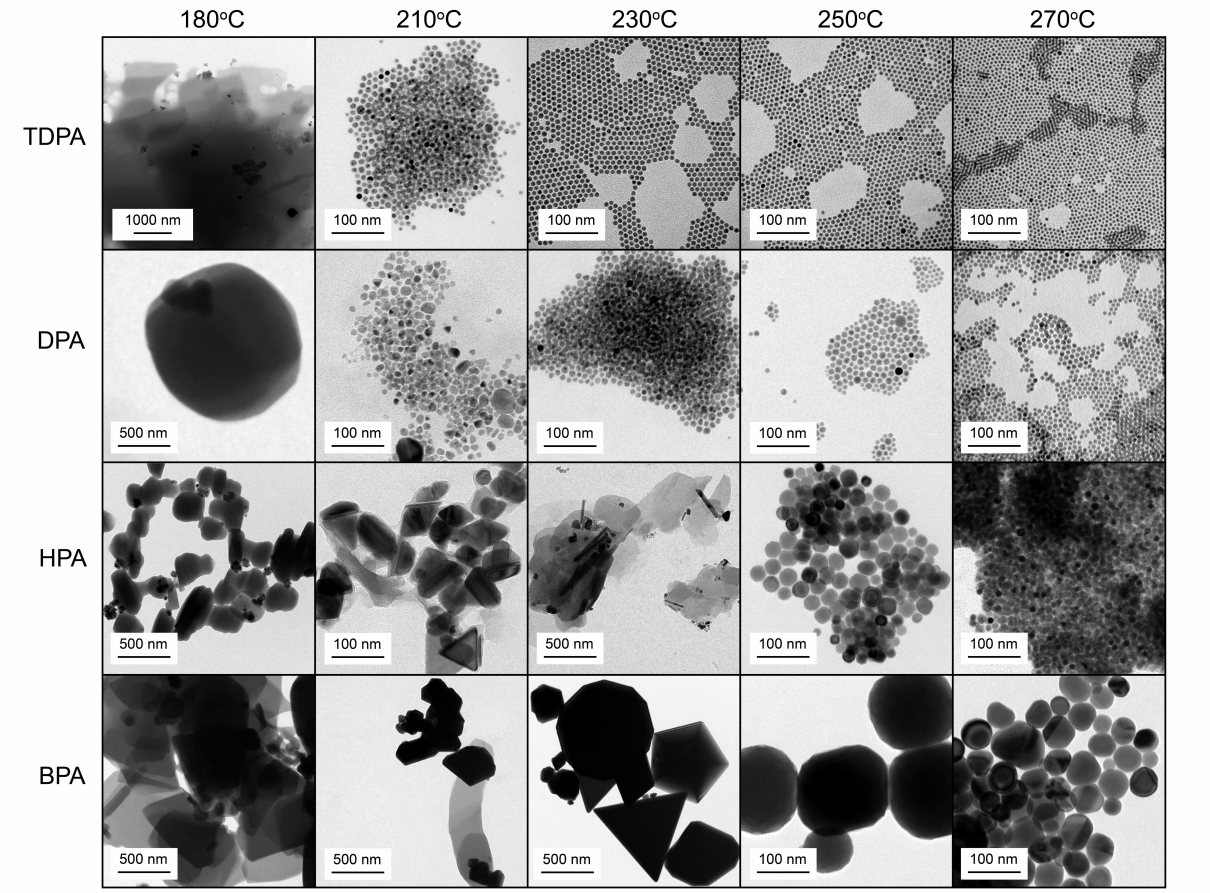


**Figure 3.** TEM images of the collected products from reactions involving Cu(OAc) and phosphonic acid ligands in TOA solvent, showing the effect of ligand tail length and reaction temperature, $T_2$.

### *Monitoring the chemical and structural transformation of the lamella intermediates via in-situ XAS and XRD*

To understand the chemical and structural changes occurring in the reaction mixture during the synthesis, we performed *in-situ* Cu K-edge X-ray absorption spectroscopy (XAS) and XRD measurements using synchrotron radiation. For these studies, a custom 3-neck flask was used, which quite accurately replicates the conditions of a typical synthesis (see **Figure S6**).

XAS provides information on the Cu oxidation state as well as the coordination geometry and can offer insight into how these evolve with time. For these experiments, the reaction temperature $T_2$ was set at 270 °C, as this is the highest limit of the syntheses studied above. The reaction with TDPA will be discussed as a representative example as the data were essentially identical for all of the phosphonic acid ligands (**Figures S7–S10**). **Figure 4A** shows that the pre-edge feature of the XAS spectrum becomes very sharp and intense during the first heating ramp to $T_1$ = 180 °C, which is when the conversion from Cu(OAc) to the lamellae

intermediates occurs. However, the energy of the peak does not change, indicating that Cu remains in the +1 oxidation state. The dramatic increase in intensity of the pre-edge XAS feature indicates that the coordination geometry in the lamellae is very different from that in the Cu(OAc) starting material. Previous work has attributed this feature to the Cu 1*s* to 4*p* electronic transition, which is very sensitive to the coordination geometry and coordination number.[56] Specifically, a sharp and intense pre-edge feature is assigned to low-coordinate Cu(I) ions, such as a linear, two-coordinate geometry or similar. In a linear geometry, the energy of the Cu $2p_z$ orbital rises due to the donated electron density from the two axial ligands, leaving the Cu $2p_{x,y}$ non-bonding orbitals lying at lower energy.[57–59] The result is a very strong absorption due to the transition from the 1*s* orbital into these low-lying orbitals.

During the second heating ramp to 270 °C, this pre-edge feature reduces in intensity and shifts to lower energy, which corresponds to the reduction from Cu(I) to Cu(0).[57,58] Specifically, this change indicates the reduction of the lamellae intermediates into metallic Cu NCs. Indeed, the final spectra in all cases matched that of pure metallic Cu very well.

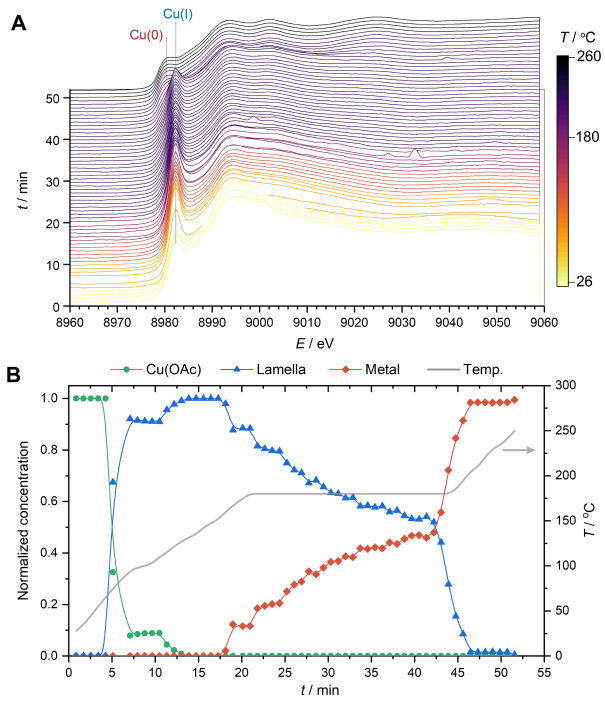


**Figure 4.** *In-situ* X-ray absorption spectroscopy data, showing (**A**) XAS spectra plotted as a function of time, revealing the conversion of Cu(OAc) to the lamella intermediate and subsequent reduction to metallic Cu – the spectra are colored according to the reaction temperature. **B**) Kinetic profile for the three principal components in the reaction, following the evolution and reduction of the lamella intermediate with time (the reaction temperature is also plotted). Reactions involving TDPA are shown as representative examples.

Deconvolution of the *in-situ* data by principal component analysis (PCA) provides a more detailed picture of the reaction as each component can be followed as a function of time (**Figures 4B, S11–S14**). We note that the extracted spectra for the lamella intermediates were identical for reactions involving different length phosphonic acid ligands, revealing identical oxidation states and coordination geometries in each reaction (**Figures S15–S18**). **Figure 4B** shows that the concentration of metallic Cu steadily increases during the temperature plateau at 180 ºC before rapidly rising during the heating ramp from 180 ºC to 270 ºC. The TEM of the lamella sheets isolated after the 180 ºC plateau revealed the presence of higher-contrast spots that are consistent with the growth of metallic clusters within or on top of the lamella (**Figure S19**). Finally, during the second heating ramp towards 270 ºC, the remainder of the lamella intermediate is rapidly converted into metallic Cu, which is coincident with the visible formation of Cu NCs in the flask *via* a yellow to brown color change of the solution.

While *in-situ* XAS studies provide insight into the changing oxidation state and coordination geometry of Cu throughout the reaction, further structural details can be obtained from *in-situ* XRD experiments. For example, structural changes in the lamella phase and their conversion into crystalline Cu can be studied. Representative *in-situ* XRD patterns are shown in **Figure 5** for the longest (TDPA) and the shortest (BPA) phosphonic acids (other data are reported in **Figures S20–S24**). For these experiments, $T_1$ and $T_2$ were set to 150 ºC and 240 ºC, respectively, to focus on the formation of anisotropic shapes. As a general trend, the lamellae phases, which are distinguishable in the low-angle region, rapidly form from Cu(OAc) during the initial heating stages and are stable for the duration of the first temperature plateau at $T_1$. The corresponding lamella *D* spacings in these *in-situ* XRD experiments are identical to those for the isolated lamellae (**Figure 1**) and depend on the length of the phosphonic acid ligand (**Figure S25**). During the second heating ramp to 240 ºC, the lamella phases convert into metallic Cu whose characteristic peaks are observed at higher angles, around 9 degrees and 11 degrees.

For the TDPA lamella (**Figure 5A**), the principal lamella peak at 0.52 degrees suddenly disappears at 180 ºC. Following this event, a scattering peak is observed at 0.42 degrees, which rapidly grows in intensity and shifts to even lower angles (minimum $2\theta = 0.35$ degrees). These changes indicate that the long-chain lamella collapses. The growth and shift of the low-angle scattering peak is accompanied by the growth of a set of very broad peaks for the metallic phase

of Cu. The sharply oscillating low-angle scattering pattern observed when the metallic Cu NCs have fully developed is consistent with the formation of small, monodisperse nanoparticles[60,61]; the product from this reaction are indeed 6 nm, monodisperse spheres.

For the BPA lamella (**Figure 5B**), the principal lamella peak at 1.24 degrees is still observable in the mixture above 230 ºC, indicating that the short-chain lamella does not collapse in the same way as the long-chain lamella. Just below this temperature, sharp Cu peaks appear very quickly in the wider-angle region, indicating the rapid formation of larger Cu NCs. The lamella phase is persistent during the Cu NC growth phase and we also note that the initial lamella peak shifts to lower angles during heating. These changes correspond to a *D*-spacing expansion from the initial 14.36 Å, to 15.57 Å at 150 ºC and to 16.78 Å at 230 ºC. This expansion may evidence the formation of small Cu clusters within the 2D lamella structure. Indeed, quasi-stable Cu clusters in the sub-nanometer regime have been studied[62,63] and similar-size clusters could be assembling laterally within the lamella template. With these nuclei supported in the lamella assembly in proximity with one another, their fusion and growth into a larger crystallite is expected to be rapid, in agreement with the rapid growth of the metallic Cu peak in the *in-situ* XRD experiment. In comparison, after the long-chain lamella collapses and the Cu ions are reduced to metallic nuclei, their growth into spherical NCs occurs much more slowly as they are dispersed in solution.

Interestingly, the temperature at which the lamellae transform into crystalline metallic Cu highly depends on the aliphatic tail length of the ligand (**Figure 5C, Figure S26**). The persistence of the lamella phase in the mixture follows a linear trend between the two extremes discussed above, with shorter-chain phosphonic acid ligands imparting greater stability on the lamella assembly and delaying the onset of Cu crystallization. The higher stability of the shorter-chain lamellae is in line with the lack of any significant interdigitation among the aliphatic chains.

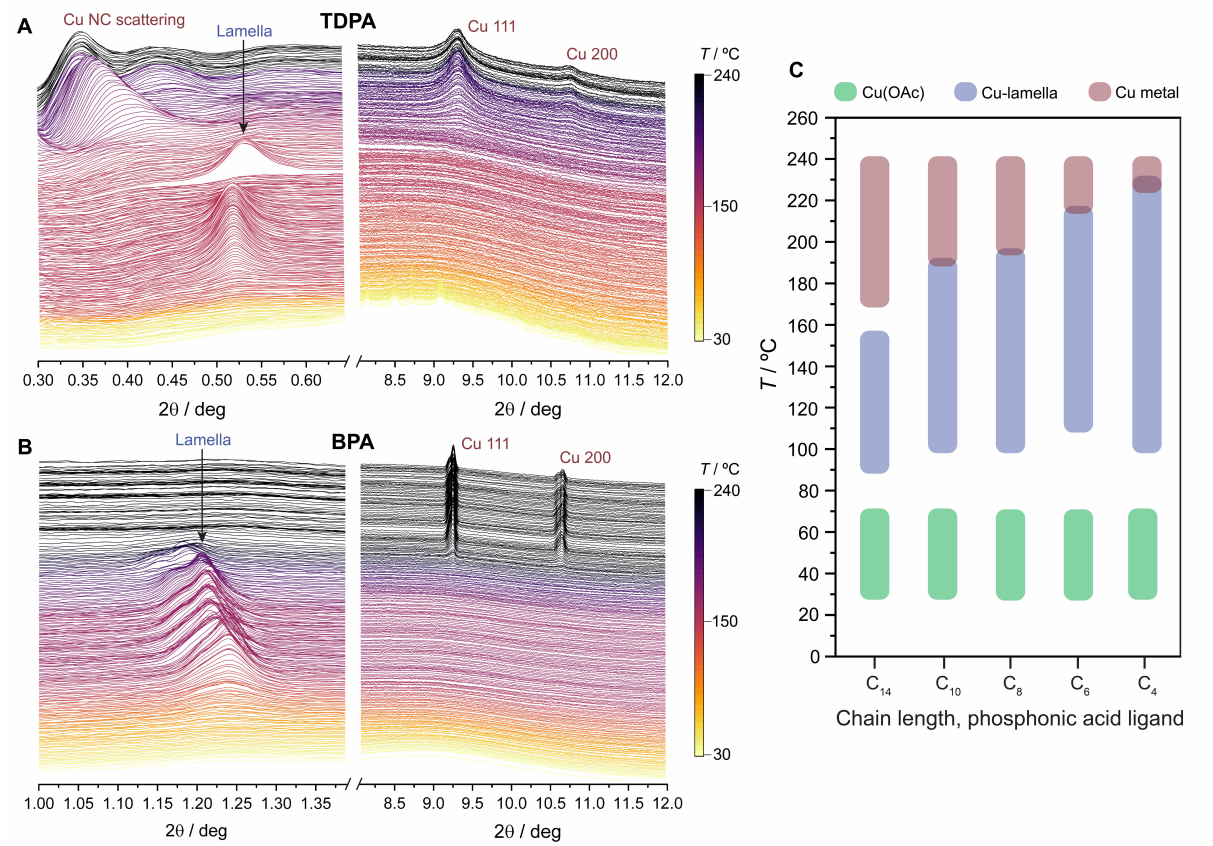


**Figure 5.** *In-situ* X-ray diffraction data, showing (**A**) the low-angle and high-angle regions for a reaction containing TDPA, Cu(OAc) and TOA, and (**B**) the low-angle and high-angle regions for a reaction containing BPA, Cu(OAc) and TOA. Lamella phases and scattering from Cu nuclei and NCs are seen in the low-angle regions while metallic phases are seen in the high-angle regions (all labelled). Diffractograms are plotted as a function of time and the reaction temperature is shown as a color map. **C**) Summary of the temperatures at which the different phases are observed, revealing the relationship between lamella stability and the phosphonic acid tail length.

### *Synthesis optimization towards 2D Cu nanostructures*

The persistence of the BPA lamellae at higher temperature during the Cu NC crystallization is the required condition that enables templating effects for the attainment of 2D structures. The Cu NCs obtained from the BPA-derived lamella at 230 ºC were promising (**Figure 3**), nevertheless they lacked uniformity in size and shape.

Inspired by previous work on lamella templating of 2D CdSe NCs[33,34,37], we attempted mild annealing of the BPA lamella at the formation temperature ($T_1$) to allow the Cu nuclei more time to fuse within the molecular template. However, this strategy was largely unsuccessful as the reduction of Cu(I) requires higher temperatures in this reaction mixture; products from these reactions contained large amounts of residual lamella (**Figure S27**). To circumvent this

issue, we attempted to promote the Cu(0) formation at lower temperature in the lamella host by introducing a reducing agent. However, injection of ascorbic acid into the BPA reaction mixture resulted in the formation of large aggregates (**Figure S28**), suggesting that the combination of strong reductants with these lamella intermediates disrupts the templating effect.

Another plausible hypothesis to explain the polydispersity in both size and shape of the BPA-derived samples is the poor colloidal stability and solubility of the BPA-lamellae themselves. The stacking of poorly dispersed lamellae could lead to aggregation of the Cu NCs upon decomposition of the template. We reasoned that improving the colloidal stability and solubility of the lamellae intermediates might impart greater homogeneity in the final NC product. Based on our previous experience, we preferred to avoid carboxylic acid ligands as they facilitate copper oxidation during the synthesis. Therefore, we opted for oleylamine (OLAM), which is a common solvent and surfactant in colloidal NC synthesis.[64] Furthermore, it could act as a mild reductant along with TOA, which is already present. Different OLAM concentrations were screened and a 1:1 molar ratio of OLAM and Cu(OAc) was found to improve the uniformity of both the lamella intermediate and Cu NC product (**Figure S29**). Heating a mixture of Cu(OAc), BPA, TOA and OLAM to 220 ºC produced a sample of Cu NCs containing 57% of anisotropic plates, 93% of which are triangles with average edge lengths of 385 nm (**Figures 6A**, **S30–S31**). Without OLAM, anisotropic shapes accounted for only 28% of the sample. The size distribution remains quite broad, yet it is improved after introducing OLAM, while the equilaterality and sharpness of the triangular Cu NCs were almost identical after introducing OLAM (**Figures S31–S32**). We highlight that the temperature of 220 ºC was chosen as the *in-situ* XRD studies revealed that the lamella template is persistent and that Cu NC reduction and crystallization can occur here (**Figure 5C**).

Selected-area electron diffraction (SAED) of a single nanoplate revealed the hexagonal patterns for the (111) and 1/3(422) reflections of the face-centered cubic structure of crystalline metallic Cu (**Figure 6B**). Note that the latter reflection is formally forbidden but is often observed in thin, 2D metallic NCs that feature stacking faults from non-3*n* layers in the crystal structure that are bound by atomically flat faces.[65–69] The periodic contrast in the HAADF-STEM image of the edge of a triangular Cu NC corresponds to the (200) planes of metallic Cu with a lattice spacing of 1.9 Å (**Figure 6C**). Finally, X-ray diffraction evidenced an intense

peak for the (111) reflection due to the preferred orientation and high ratio of the (111) facet presented by the triangular Cu NCs (**Figure 6D**).

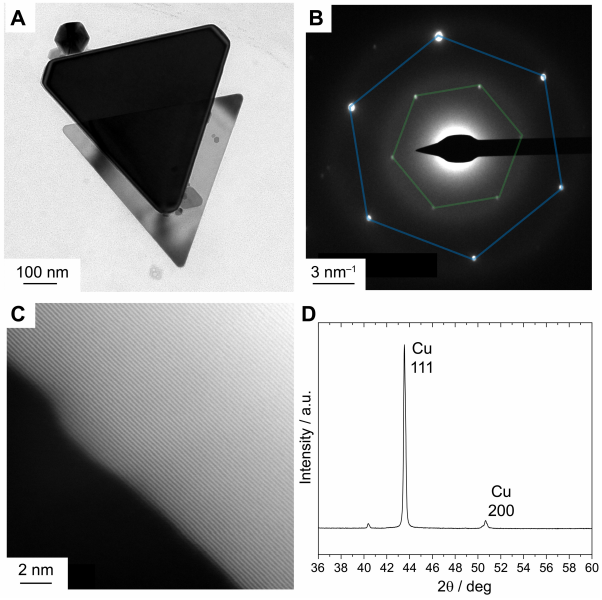


**Figure 6. A**) Bright-field TEM image of anisotropic Cu NCs synthesized from lamella templates. **B**) SAED image for a single triangular Cu NC, showing the forbidden 1/3(422) reflection (highlighted in green) and the (111) reflection (highlighted in blue). **C**) HAADF-STEM image of the edge of a triangular Cu NC. **D**) XRD pattern for the anisotropic Cu NCs, showing the preferential orientation of the (111) facet, which arises mainly from triangular Cu NCs.

Copper nanowires and nanosheets have previously been synthesized through selective capping of the (111) facet[65,70,71], thus OLAM could conceivably be implicated in a similar role. However, only the unique combination of BPA, which forms thermally stable lamellae, and OLAM results in a higher yield of triangular plates. In contrast, when OLAM was employed in combination with TDPA, monodisperse, spherical Cu NCs were still obtained from the reaction (**Figure S33**), thereby ruling out the anisotropic NC growth by capping of the (111) facet.

Additional *in-situ* XRD measurements evidenced that OLAM is not incorporated into the lamella structure and does not impact the structural transformations during the reaction (**Figures S34–S41**). TEM characterization of the BPA-lamella intermediates in the presence of OLAM (**Figure S42A**) revealed that small, spherical Cu crystalline domains are present at 150 °C, which is consistent with the hypothesis of Cu nuclei forming within the lamellae. The most striking difference between the BPA-lamella intermediates formed in the absence and in

the presence of OLAM is that the latter are uniform and well-assembled circular lamella sheets (**Figure S42B**) and possess an improved colloidal stability compared to those obtained without OLAM. In the synthesis of metal NCs, including Cu NCs, using reverse micelles, Pileni *et al.* have shown that metal clusters form within inverse micelles and have attempted to correlate the micelle shapes to the shapes of the obtained NCs, although this correlation remains controversial and debated.[72–75] Similarly, while the observation that uniform and well-assembled circular lamella sheets form in the presence of BPA and OLAM is intriguing, we acknowledge that the final NC shape is not necessarily dictated by the shape of the lamella intermediate. However, we do suggest that the improved colloidal stability of the intermediates is important to increase the yield of the triangular plates.

***Mechanistic insight in the lamella-assisted synthesis of Cu NCs***

From all of the above discussions, we confidently propose the mechanistic picture that is illustrated in **Figure 7**. Copper-phosphonate lamellae forming from long-chain phosphonic acids decompose rapidly and release well-dispersed nuclei that go on to form monodisperse spheres. In contrast, short-chain lamellae are more thermally robust than long-chain lamellae, thus their structure persists during the Cu(I) reduction step into the Cu(0) nuclei and direct the growth of the resulting Cu NCs towards anisotropic shapes. Furthermore, we have learned that improving the dispersibility of the short-chain lamella intermediates in the reaction medium plays an important role in improving the size and shape homogeneity of the final product towards mostly triangular plates. Long chain primary amines emerged as suitable reagents to realize this condition.

In other studies, the final shape of metal NCs has been connected to seeds of specific shapes; for example, triangular plates should grow from plate seeds with stacking faults.[76] In this work, triangular Cu plates have been synthesized, yet the smallest observable Cu particles are roughly spherical and single crystal. This result demonstrates that the requirement for targeting specific seed shapes can be bypassed by directing the anisotropic growth of spherical seeds with a templating reaction intermediate.

Follow-up studies are still needed to further understand the evolution of the cooperative organization of inorganic and organic molecular species during the nucleation and growth of the Cu clusters within the lamella framework. These studies should help us to better ascertain whether the Cu clusters truly grow within the layers of the coordination polymer, or whether

regions of the lamellae break down into Cu clusters that rapidly grow with a lateral preference. The investigation of these dynamic phenomena is not trivial. However, they are important to guide further optimization of the synthesis towards higher yields of anisotropic Cu NCs. *In-situ* nuclear magnetic resonance spectroscopy might be one of the most suitable techniques to consider in the future.[77]

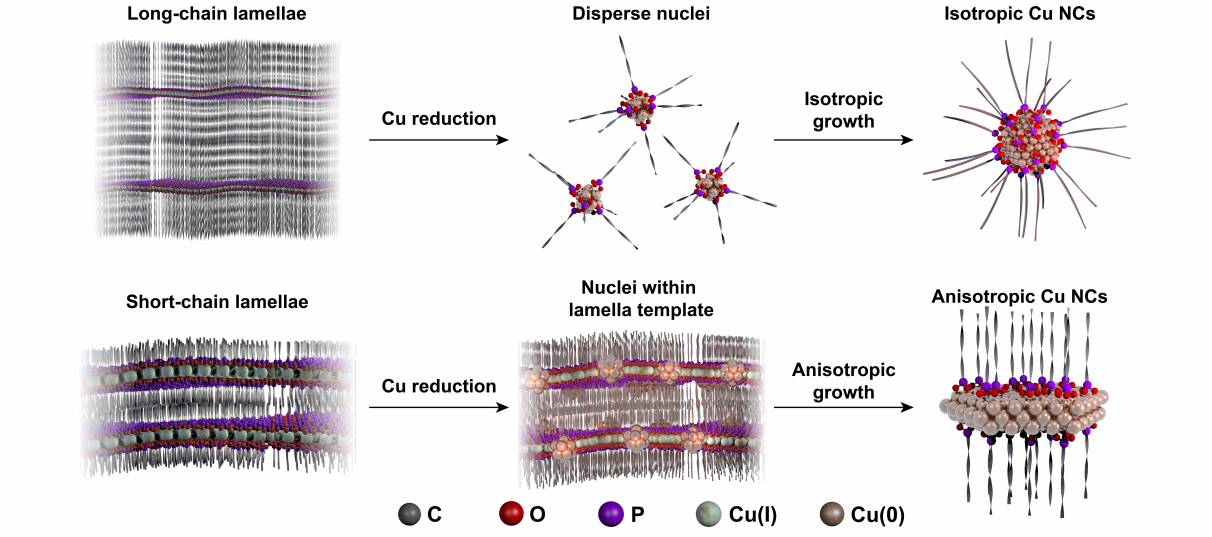


**Figure 7.** Schematic illustration of lamella-assisted synthesis of Cu NCs for achieving shape control. Short-chain lamellae are thermally stable at the reduction temperature, allowing templated nucleation, leading to anisotropic NC growth.

## Conclusions

In conclusion, we have studied the synthesis of Cu NCs *via* Cu(I)-phosphonate lamella intermediates by using different length aliphatic phosphonic acid ligands. We have discovered that the chain length of the ligands determines the structure of the lamellae and, thus, their decomposition temperature. With this new knowledge, we have demonstrated that anisotropic Cu NCs, mostly triangular plates, form from the more thermally robust short-chain lamellae. On the contrary, spherical Cu NCs are the reaction product of the long-chain lamellae.

This study highlights that the rational selection of organic ligands during colloidal NC synthesis should take all of their roles in the reaction into account, which goes beyond their most trivial function as surface passivating agents on the NCs during their formation.

Finally, we envision that the future development of using lamellae as well-defined pre-nucleation intermediates will allow even greater control in NC synthesis, especially for non-

noble metal NCs. For example, being able to synthesize metallic nanosheets with tunable thickness and being able to tune the elemental composition by combining lamellae of different transition metals will greatly advance their use in catalytic and energy applications.[32–40]

**Notes.**

The authors declare no competing financial interest.

The data underlying this study are openly available in Zenodo at https://doi.org/10.5281/zenodo.6362954.

**Acknowledgments**

This worked was primarily financed by the H2020 Marie Curie Individual Fellowship grant SURFCAT with agreement number 837378 and contribution from the European Research Council (ERC) under the European Union's Horizon 2020 research and innovation program (grant agreement no. 715634-HYCAT) L.C.-A. and P.A. thank the Swiss National Science Foundation (SNSF) for financial support from grant number 200021L_191997/1 and from the NCCR Catalysis (grant number 180544), a National Centre of Competence in Research funded by the Swiss National Science Foundation, respectively. The authors thank the European Synchrotron Radiation Facility in Grenoble, France for the provision of synchrotron radiation beamtime at the Swiss-Norwegian beamline BM31 and thank Dr Wouter van Beek for assistance.

**References**

(1) Talapin, D. V.; Lee, J.-S.; Kovalenko, M. V.; Shevchenko, E. V. Prospects of Colloidal Nanocrystals for Electronic and Optoelectronic Applications. *Chem. Rev.* **2010**, *110*, 389–458.

(2) Parak, W. J.; Gerion, D.; Pellegrino, T.; Zanchet, D.; Micheel, C.; Williams, S. C.; Boudreau, R.; Gros, M. A. L.; Larabell, C. A.; Alivisatos, A. P. Biological Applications of Colloidal Nanocrystals. *Nanotechnology* **2003**, *14*, R15–R27.

(3) Guntern, Y. T.; Okatenko, V.; Pankhurst, J.; Varandili, S. B.; Iyengar, P.; Koolen, C.; Stoian, D.; Vavra, J.; Buonsanti, R. Colloidal Nanocrystals as Electrocatalysts with Tunable Activity and Selectivity. *ACS Catal.* **2021**, 1248–1295.

(4) Cargnello, M. Colloidal Nanocrystals as Building Blocks for Well-Defined Heterogeneous Catalysts. *Chem. Mater.* **2019**, *31*, 576–596.

(5) Shi, Y.; Lyu, Z.; Zhao, M.; Chen, R.; Nguyen, Q. N.; Xia, Y. Noble-Metal Nanocrystals with Controlled Shapes for Catalytic and Electrocatalytic Applications. *Chem. Rev.* **2021**, *121*, 649–735.

(6) Kwon, S. G.; Hyeon, T. Formation Mechanisms of Uniform Nanocrystals via Hot-Injection and Heat-Up Methods. *Small* **2011**, *7*, 2685–2702.

(7) Mantella, V.; Castilla-Amorós, L.; Buonsanti, R. Shaping Non-Noble Metal Nanocrystals *via* Colloidal Chemistry. *Chem. Sci.* **2020**, *11*, 11394–11403.

(8) Yang, T.; Shi, Y.; Janssen, A.; Xia, Y. Surface Capping Agents and Their Roles in Shape-Controlled Synthesis of Colloidal Metal Nanocrystals. *Angew. Chem. Int. Ed.* **2020**, *59*, 15378–15401.

(9) Park, J.; Joo, J.; Kwon, S. G.; Jang, Y.; Hyeon, T. Synthesis of Monodisperse Spherical Nanocrystals. *Angew. Chem. Int. Ed.* **2007**, *46*, 4630–4660.

(10) Lee, J.; Yang, J.; Kwon, S. G.; Hyeon, T. Nonclassical Nucleation and Growth of Inorganic Nanoparticles. *Nat. Rev. Mater.* **2016**, *1*, 16034.

(11) Loiudice, A.; Buonsanti, R. Reaction Intermediates in the Synthesis of Colloidal Nanocrystals. *Nat. Synth.* **2022**, *just accepted*.

(12) Lee, H.; Yoon, D.-E.; Koh, S.; Kang, M. S.; Lim, J.; Lee, D. C. Ligands as a Universal Molecular Toolkit in Synthesis and Assembly of Semiconductor Nanocrystals. *Chem. Sci.* **2020**, *11*, 2318–2329.

(13) Heuer-Jungemann, A.; Feliu, N.; Bakaimi, I.; Hamaly, M.; Alkilany, A.; Chakraborty, I.; Masood, A.; Casula, M. F.; Kostopoulou, A.; Oh, E.; Susumu, K.; Stewart, M. H.; Medintz, I. L.; Stratakis, E.; Parak, W. J.; Kanaras, A. G. The Role of Ligands in the Chemical Synthesis and Applications of Inorganic Nanoparticles. *Chem. Rev.* **2019**, *119*, 4819–4880.

(14) Lazzari, S.; Theiler, P. M.; Shen, Y.; Coley, C. W.; Stemmer, A.; Jensen, K. F. Ligand-Mediated Nanocrystal Growth. *Langmuir* **2018**, *34*, 3307–3315.

(15) Yin, Y.; Alivisatos, A. P. Colloidal Nanocrystal Synthesis and the Organic–Inorganic Interface. *Nature* **2005**, *437*, 664–670.

(16) Bealing, C. R.; Baumgardner, W. J.; Choi, J. J.; Hanrath, T.; Hennig, R. G. Predicting Nanocrystal Shape through Consideration of Surface-Ligand Interactions. *ACS Nano* **2012**, *6*, 2118–2127.

(17) Huo, D.; Kim, M. J.; Lyu, Z.; Shi, Y.; Wiley, B. J.; Xia, Y. One-Dimensional Metal Nanostructures: From Colloidal Syntheses to Applications. *Chem. Rev.* **2019**, *119*, 8972–9073.

(18) Mozaffari, S.; Li, W.; Thompson, C.; Ivanov, S.; Seifert, S.; Lee, B.; Kovarik, L.; Karim, A. M. Colloidal Nanoparticle Size Control: Experimental and Kinetic Modeling Investigation of the Ligand–Metal Binding Role in Controlling the Nucleation and Growth Kinetics. *Nanoscale* **2017**, *9*, 13772–13785.

(19) Ortiz, N.; Skrabalak, S. E. On the Dual Roles of Ligands in the Synthesis of Colloidal Metal Nanostructures. *Langmuir* **2014**, *30*, 6649–6659.

(20) Niu, Z.; Peng, Q.; Gong, M.; Rong, H.; Li, Y. Oleylamine-Mediated Shape Evolution of Palladium Nanocrystals. *Angew. Chem. Int. Ed.* **2011**, *50*, 6315–6319.

(21) Abécassis, B.; Testard, F.; Spalla, O.; Barboux, P. Probing in Situ the Nucleation and Growth of Gold Nanoparticles by Small-Angle X-Ray Scattering. *Nano Lett.* **2007**, *7*, 1723–1727.

(22) Strach, M.; Mantella, V.; Pankhurst, J. R.; Iyengar, P.; Loiudice, A.; Das, S.; Corminboeuf, C.; van Beek, W.; Buonsanti, R. Insights into Reaction Intermediates to Predict Synthetic Pathways for Shape-Controlled Metal Nanocrystals. *J. Am. Chem. Soc.* **2019**, *141*, 16312–16322.

(23) Gary, D. C.; Terban, M. W.; Billinge, S. J. L.; Cossairt, B. M. Two-Step Nucleation and Growth of InP Quantum Dots via Magic-Sized Cluster Intermediates. *Chem. Mater.* **2015**, *27*, 1432–1441.

(24) Niu, J.; Wang, D.; Qin, H.; Xiong, X.; Tan, P.; Li, Y.; Liu, R.; Lu, X.; Wu, J.; Zhang, T.; Ni, W.; Jin, J. Novel Polymer-Free Iridescent Lamellar Hydrogel for Two-Dimensional Confined Growth of Ultrathin Gold Membranes. *Nat. Commun.* **2014**, *5*, 3313.

(25) Nagle, J. F.; Tristram-Nagle, S. Structure of Lipid Bilayers. *Biochim. Biophys. Acta BBA - Rev. Biomembr.* **2000**, *1469*, 159–195.

(26) Moradi, S.; Nowroozi, A.; Shahlaei, M. Shedding Light on the Structural Properties of Lipid Bilayers Using Molecular Dynamics Simulation: A Review Study. *RSC Adv.* **2019**, *9*, 4644–4658.

(27) Shahane, G.; Ding, W.; Palaiokostas, M.; Orsi, M. Physical Properties of Model Biological Lipid Bilayers: Insights from All-Atom Molecular Dynamics Simulations. *J. Mol. Model.* **2019**, *25*, 76.

(28) Park, S.-H.; Lee, Y.-J.; Huh, Y.-D. Inorganic–Organic Chain Assemblies as Lamellar Nanoreactors for Growing One-Dimensional $Cu(OH)_2$ and CuO Nanostructures. *Chem. Commun.* **2011**, *47*, 11763.

(29) Gromova, M.; Lefrançois, A.; Vaure, L.; Agnese, F.; Aldakov, D.; Maurice, A.; Djurado, D.; Lebrun, C.; de Geyer, A.; Schülli, T. U.; Pouget, S.; Reiss, P. Growth Mechanism and Surface State of $CuInS_2$ Nanocrystals Synthesized with Dodecanethiol. *J. Am. Chem. Soc.* **2017**, *139*, 15748–15759.

(30) Loubat, A.; Lacroix, L.-M.; Robert, A.; Impéror-Clerc, M.; Poteau, R.; Maron, L.; Arenal, R.; Pansu, B.; Viau, G. Ultrathin Gold Nanowires: Soft-Templating versus Liquid Phase Synthesis, a Quantitative Study. *J. Phys. Chem. C* **2015**, *119*, 4422–4430.

(31) Mantella, V.; Strach, M.; Frank, K.; Pankhurst, J. R.; Stoian, D.; Gadiyar, C.; Nickel, B.; Buonsanti, R. Polymer Lamellae as Reaction Intermediates in the Formation of Copper Nanospheres as Evidenced by In Situ X-ray Studies. *Angew. Chem. Int. Ed.* **2020**, *59*, 11627–11633.

(32) Bryks, W.; Smith, S. C.; Tao, A. R. Metallomesogen Templates for Shape Control of Metal Selenide Nanocrystals. *Chem. Mater.* **2017**, *29*, 3653–3662.

(33) Son, J. S.; Wen, X.-D.; Joo, J.; Chae, J.; Baek, S.; Park, K.; Kim, J. H.; An, K.; Yu, J. H.; Kwon, S. G.; Choi, S.-H.; Wang, Z.; Kim, Y.-W.; Kuk, Y.; Hoffmann, R.; Hyeon, T. Large-Scale Soft

Colloidal Template Synthesis of 1.4 nm Thick CdSe Nanosheets. *Angew. Chem. Int. Ed.* **2009**, *48*, 6861–6864.

(34) Baek, W.; Bootharaju, M. S.; Walsh, K. M.; Lee, S.; Gamelin, D. R.; Hyeon, T. Highly Luminescent and Catalytically Active Suprastructures of Magic-Sized Semiconductor Nanoclusters. *Nat. Mater.* **2021**, *20*, 650–657.

(35) Zhang, X.; Zhang, J.; Zhao, J.; Pan, B.; Kong, M.; Chen, J.; Xie, Y. Half-Metallic Ferromagnetism in Synthetic $Co_9Se_8$ Nanosheets with Atomic Thickness. *J. Am. Chem. Soc.* **2012**, *134*, 11908–11911.

(36) Bryks, W.; Lupi, E.; Ngo, C.; Tao, A. R. Digenite Nanosheets Synthesized by Thermolysis of Layered Copper-Alkanethiolate Frameworks. *J. Am. Chem. Soc.* **2016**, *138*, 13717–13725.

(37) Baek, W.; Bootharaju, M. S.; Lorenz, S.; Lee, S.; Stolte, S.; Fainblat, R.; Bacher, G.; Hyeon, T. Nanoconfinement-Controlled Synthesis of Highly Active, Multinary Nanoplatelet Catalysts from Lamellar Magic-Sized Nanocluster Templates. *Adv. Funct. Mater.* **2021**, *31*, 2107447.

(38) Wang, F.; Wang, Y.; Liu, Y.-H.; Morrison, P. J.; Loomis, R. A.; Buhro, W. E. Two-Dimensional Semiconductor Nanocrystals: Properties, Templated Formation, and Magic-Size Nanocluster Intermediates. *Acc. Chem. Res.* **2015**, *48*, 13–21.

(39) Liu, Y.-H.; Wang, F.; Wang, Y.; Gibbons, P. C.; Buhro, W. E. Lamellar Assembly of Cadmium Selenide Nanoclusters into Quantum Belts. *J. Am. Chem. Soc.* **2011**, *133*, 17005–17013.

(40) Wang, Y.; Zhang, Y.; Wang, F.; Giblin, D. E.; Hoy, J.; Rohrs, H. W.; Loomis, R. A.; Buhro, W. E. The Magic-Size Nanocluster $(CdSe)_{34}$ as a Low-Temperature Nucleant for Cadmium Selenide Nanocrystals; Room-Temperature Growth of Crystalline Quantum Platelets. *Chem. Mater.* **2014**, *26*, 2233–2243.

(41) Huang, J.; Buonsanti, R. Colloidal Nanocrystals as Heterogeneous Catalysts for Electrochemical $CO_2$ Conversion. *Chem. Mater.* **2019**, *31*, 13–25.

(42) Iyengar, P.; Huang, J.; De Gregorio, G. L.; Gadiyar, C.; Buonsanti, R. Size Dependent Selectivity of Cu Nano-Octahedra Catalysts for the Electrochemical Reduction of $CO_2$ to $CH_4$. *Chem. Commun.* **2019**, *55*, 8796–8799.

(43) De Gregorio, G. L.; Burdyny, T.; Loiudice, A.; Iyengar, P.; Smith, W. A.; Buonsanti, R. Facet-Dependent Selectivity of Cu Catalysts in Electrochemical $CO_2$ Reduction at Commercially Viable Current Densities. *ACS Catal.* **2020**, *10*, 4854–4862.

(44) Reske, R.; Mistry, H.; Behafarid, F.; Roldan Cuenya, B.; Strasser, P. Particle Size Effects in the Catalytic Electroreduction of $CO_2$ on Cu Nanoparticles. *J. Am. Chem. Soc.* **2014**, *136*, 6978–6986.

(45) Manthiram, K.; Beberwyck, B. J.; Alivisatos, A. P. Enhanced Electrochemical Methanation of Carbon Dioxide with a Dispersible Nanoscale Copper Catalyst. *J. Am. Chem. Soc.* **2014**, *136*, 13319–13325.

(46) Loiudice, A.; Lobaccaro, P.; Kamali, E. A.; Thao, T.; Huang, B. H.; Ager, J. W.; Buonsanti, R. Tailoring Copper Nanocrystals towards $C_2$ Products in Electrochemical $CO_2$ Reduction. *Angew. Chem. Int. Ed.* **2016**, *55*, 5789–5792.

(47) Kim, D.; Kley, C. S.; Li, Y.; Yang, P. Copper Nanoparticle Ensembles for Selective Electroreduction of $CO_2$ to $C_2$–$C_3$ Products. *Proc. Natl. Acad. Sci.* **2017**, *114*, 10560–10565.

(48) Osowiecki, W. T.; Nussbaum, J. J.; Kamat, G. A.; Katsoukis, G.; Ledendecker, M.; Frei, H.; Bell, A. T.; Alivisatos, A. P. Factors and Dynamics of Cu Nanocrystal Reconstruction under $CO_2$ Reduction. *ACS Appl. Energy Mater.* **2019**, *2*, 7744–7749.

(49) Xie, Y. P.; Liu, G.; Yin, L.; Cheng, H.-M. Crystal Facet-Dependent Photocatalytic Oxidation and Reduction Reactivity of Monoclinic $WO_3$ for Solar Energy Conversion. *J. Mater. Chem.* **2012**, *22*, 6746.

(50) Shi, M.; Li, G.; Li, J.; Jin, X.; Tao, X.; Zeng, B.; Pidko, E. A.; Li, R.; Li, C. Intrinsic Facet-Dependent Reactivity of Well-Defined BiOBr Nanosheets on Photocatalytic Water Splitting. *Angew. Chem. Int. Ed.* **2020**, *59*, 6590–6595.

(51) Luo, W.; Nie, X.; Janik, M. J.; Asthagiri, A. Facet Dependence of $CO_2$ Reduction Paths on Cu Electrodes. *ACS Catal.* **2016**, *6*, 219–229.

(52) Iyengar, P.; Kolb, M. J.; Pankhurst, J. R.; Calle-Vallejo, F.; Buonsanti, R. Elucidating the Facet-Dependent Selectivity for $CO_2$ Electroreduction to Ethanol of Cu–Ag Tandem Catalysts. *ACS Catal.* **2021**, *11*, 4456–4463.

(53) Sarkar, R.; Gowd, E. B.; Ramakrishnan, S. Precise Control of Grafting Density in Periodically Grafted Amphiphilic Copolymers: An Alternate Strategy to Fine-Tune the Lamellar Spacing in the Sub-10 nm Regime. *Polym. Chem.* **2020**, *11*, 4143–4154.

(54) de Pauli, M.; Prado, M. de C.; Matos, M. J. S.; Fontes, G. N.; Perez, C. A.; Mazzoni, M. S. C.; Neves, B. R. A.; Malachias, A. Thermal Stability and Ordering Study of Long- and Short-Alkyl Chain Phosphonic Acid Multilayers. *Langmuir* **2012**, *28*, 15124–15133.

(55) de Pauli, M.; Magalhães-Paniago, R.; Malachias, A. Phase-Dependent Premelting of Self-Assembled Phosphonic Acid Multilayers. *Phys. Rev. E* **2013**, *87*, 052402.

(56) Oyanagi, H.; Orimoto, Y.; Hayakawa, K.; Hatada, K.; Sun, Z.; Zhang, L.; Yamashita, K.; Nakamura, H.; Uehara, M.; Fukano, A.; Maeda, H. Nanoclusters Synthesized by Synchrotron Radiolysis in Concert with Wet Chemistry. *Sci. Rep.* **2015**, *4*, 7199.

(57) Kau, L. S.; Spira-Solomon, D. J.; Penner-Hahn, J. E.; Hodgson, K. O.; Solomon, E. I. X-Ray Absorption Edge Determination of the Oxidation State and Coordination Number of Copper. Application to the Type 3 Site in Rhus Vernicifera Laccase and Its Reaction with Oxygen. *J. Am. Chem. Soc.* **1987**, *109*, 6433–6442.

(58) Rudolph, J.; Jacob, C. R. Revisiting the Dependence of Cu K-Edge X-Ray Absorption Spectra on Oxidation State and Coordination Environment. *Inorg. Chem.* **2018**, *57*, 10591–10607.

(59) Baker, M. L.; Mara, M. W.; Yan, J. J.; Hodgson, K. O.; Hedman, B.; Solomon, E. I. K- and L-Edge X-Ray Absorption Spectroscopy (XAS) and Resonant Inelastic X-Ray Scattering (RIXS) Determination of Differential Orbital Covalency (DOC) of Transition Metal Sites. *Coord. Chem. Rev.* **2017**, *345*, 182–208.

(60) Borchert, H.; Shevchenko, E. V.; Robert, A.; Mekis, I.; Kornowski, A.; Grübel, G.; Weller, H. Determination of Nanocrystal Sizes: A Comparison of TEM, SAXS, and XRD Studies of Highly Monodisperse $CoPt_3$ Particles. *Langmuir* **2005**, *21*, 1931–1936.

(61) Chen, X.; Wang, J.; Pan, R.; Roth, S.; Förster, S. Insights into Growth Kinetics of Colloidal Gold Nanoparticles: In Situ SAXS and UV–Vis Evaluation. *J. Phys. Chem. C* **2021**, *125*, 1087–1095.

(62) Salorinne, K.; Chen, X.; Troff, R. W.; Nissinen, M.; Häkkinen, H. One-Pot Synthesis and Characterization of Subnanometre-Size Benzotriazolate Protected Copper Clusters. *Nanoscale* **2012**, *4*, 4095.

(63) Wei, W.; Lu, Y.; Chen, W.; Chen, S. One-Pot Synthesis, Photoluminescence, and Electrocatalytic Properties of Subnanometer-Sized Copper Clusters. *J. Am. Chem. Soc.* **2011**, *133*, 2060–2063.

(64) Mourdikoudis, S.; Liz-Marzán, L. M. Oleylamine in Nanoparticle Synthesis. *Chem. Mater.* **2013**, *25*, 1465–1476.

(65) Luc, W.; Fu, X.; Shi, J.; Lv, J.-J.; Jouny, M.; Ko, B. H.; Xu, Y.; Tu, Q.; Hu, X.; Wu, J.; Yue, Q.; Liu, Y.; Jiao, F.; Kang, Y. Two-Dimensional Copper Nanosheets for Electrochemical Reduction of Carbon Monoxide to Acetate. *Nat. Catal.* **2019**, *2*, 423–430.

(66) Sun, Y.; Xia, Y. Triangular Nanoplates of Silver: Synthesis, Characterization, and Use as Sacrificial Templates For Generating Triangular Nanorings of Gold. *Adv. Mater.* **2003**, *15*, 695–699.

(67) Jiang, L.-P.; Xu, S.; Zhu, J.-M.; Zhang, J.-R.; Zhu, J.-J.; Chen, H.-Y. Ultrasonic-Assisted Synthesis of Monodisperse Single-Crystalline Silver Nanoplates and Gold Nanorings. *Inorg. Chem.* **2004**, *43*, 5877–5883.

(68) Germain, V.; Li, J.; Ingert, D.; Wang, Z. L.; Pileni, M. P. Stacking Faults in Formation of Silver Nanodisks. *J. Phys. Chem. B* **2003**, *107*, 8717–8720.

(69) Shankar, S. S.; Rai, A.; Ankamwar, B.; Singh, A.; Ahmad, A.; Sastry, M. Biological Synthesis of Triangular Gold Nanoprisms. *Nat. Mater.* **2004**, *3*, 482–488.

(70) Kim, M. J.; Alvarez, S.; Chen, Z.; Fichthorn, K. A.; Wiley, B. J. Single-Crystal Electrochemistry Reveals Why Metal Nanowires Grow. *J. Am. Chem. Soc.* **2018**, *140*, 14740–14746.

(71) Kim, M. J.; Flowers, P. F.; Stewart, I. E.; Ye, S.; Baek, S.; Kim, J. J.; Wiley, B. J. Ethylenediamine Promotes Cu Nanowire Growth by Inhibiting Oxidation of Cu(111). *J. Am. Chem. Soc.* **2017**, *139*, 277–284.

(72) Tanori, J.; Pileni, M. P. Control of the Shape of Copper Metallic Particles by Using a Colloidal System as Template. *Langmuir* **1997**, *13*, 639–646.

(73) Lisiecki, I.; Pileni, M. P. Synthesis of Copper Metallic Clusters Using Reverse Micelles as Microreactors. *J. Am. Chem. Soc.* **1993**, *115*, 3887–3896.

(74) Tanori, J.; Paule Pileni, M. Change in the Shape of Copper Nanoparticles in Ordered Phases. *Adv. Mater.* **1995**, *7*, 862–864.

(75) Pileni, M.-P. The Role of Soft Colloidal Templates in Controlling the Size and Shape of Inorganic Nanocrystals. *Nat. Mater.* **2003**, *2*, 145–150.

(76) Xia, Y.; Xiong, Y.; Lim, B.; Skrabalak, S. E. Shape-Controlled Synthesis of Metal Nanocrystals: Simple Chemistry Meets Complex Physics? *Angew. Chem. Int. Ed.* **2009**, *48*, 60–103.

(77) Firouzi, A.; Kumar, D.; Bull, L. M.; Besier, T.; Sieger, P.; Huo, Q.; Walker, S. A.; Zasadzinski, J. A.; Glinka, C.; Nicol, J.; Margolese, D.; Stucky, G. D.; Chmelka, B. F. Cooperative Organization of Inorganic-Surfactant and Biomimetic Assemblies. *Science* **1995**, *267*, 1138–1143.